Published in final edited form as:
Magn Reson Imaging. 2012 February ; 30(2): 290–298. doi:10.1016/j.mri.2011.09.022.

A dual-tuned quadrature volume coil with mixed λ/2 and λ/4 microstrip resonators for multinuclear MRSI at 7T

Yong Pang[1], **Zhentian Xie**[1], **Duan Xu**[1], **Douglas A. Kelley**[2], **Sarah J. Nelson**[1,3], **Daniel B. Vigneron**[1,3], and **Xiaoliang Zhang**[1,3,*]

[1]Department of Radiology and Biomedical Imaging, University of California San Francisco, San Francisco, CA, United States

[2]GE Healthcare, San Francisco, CA, United States

[3]UCSF/UC Berkeley Joint Graduate Group in Bioengineering, San Francisco & Berkeley, CA, United States

Abstract

In this work, an 8-element by 8-element dual-tuned quadrature volume coil with a mix of capacitor terminated half-wavelength (λ/2) and quarter-wavelength (λ/4) microstrip resonators is proposed for multinuclear MRI/S studies at 7T. In the proton channel, λ/2 microstrip resonators with capacitive terminations on both ends are employed for operation at higher frequency of 298.1 MHz; in the heteronucleus channel, capacitor terminated λ/4 resonators, suitable for low frequency operations, are used to meet the low frequency requirement. This mixed structure design is particularly advantageous for high field heteronuclei MR applications with large difference in Larmor frequency of the nuclei in question. The proposed design method makes it much easier to perform frequency tuning for heteronucleus channel using a variable capacitor with a practical capacitance range. As an example, a dual-tuned volume coil for $^{1}H/^{13}C$ mouse spectroscopic imaging was proposed to demonstrate the feasibility of this method. The finite-difference time-domain (FDTD) method is first used to model this dual-tuned volume coil and calculate the B_1 field distributions at two frequencies. Transmission parameters (S_{21}) measured between the proton channel and the carbon channel are −50 dB at 75 MHz and −35 dB at 298 MHz, showing the excellent isolation between the two channels at 7T. The proton image and ^{13}C FID CSI image of a corn oil phantom on the axial plane at 7T demonstrate the feasibility of the proposed method. A preliminary proton image of a mouse on the sagittal plane is also acquired using the proposed dual-tuned volume coil at 7T, illustrating a fairly uniform B_1 field and sufficient image coverage for imaging in mice.

Keywords

Dual-tuned; Microstrip; Volume coil; 7T; mouse imaging; MRI/S

*Corresponding author: Xiaoliang Zhang, Ph.D., Department of Radiology and Biomedical Imaging, University of California San Francisco, Byers Hall, Room 102, 1700 4th Street, San Francisco, CA94158-2330, USA, 1-415-514-4801 (Tel.), 1-415-514-4451 (Fax), xiaoliang.zhang@radiology.ucsf.edu.
Y.P. and Z.X. contributed equally to this work.

1. Introduction

Due to low natural abundance of heteronuclei, leading to low signal intensity, multinuclear MR applications, such as $^{1}H/^{13}C$ [1–5], $^{1}H/^{23}Na$ [6–8] and $^{1}H/^{31}P$ [9–12] spectroscopic imaging that are capable of depicting metabolic process in vivo, have brought forward urgent demand for efficient double-frequency RF coils to utmost detect the MR signals. Dual-tuned RF coils have been designed using different techniques such as lumped element method [13–18] and transverse electromagnetic resonator (TEM) technique [19–21], and have demonstrated great advantages in multinuclear spectroscopic imaging. However, involvement of two independently controlled frequencies makes the design of dual-tuned RF coils complicated and technically challenging, particularly at high and ultrahigh fields due to the required high frequency [22]. The high operation frequency of the ultrahigh field MR results in the increased conductor/radiation losses, degraded quality factors, augmented electromagnetic interactions between the two resonant frequencies, and difficulties in achieving required high resonant frequency of RF coils. These problems are more prominent in the presence of a living animal loaded to RF coils.

In recent years, it has been demonstrated that microstrip transmission line (MTL) RF coils are advantageous to high field in vivo MR applications with high quality factor, high frequency operation capability, reduced radiation losses, and thus improved MR sensitivity. This technique has been successfully applied to designs of surface coils [23,24], volume coils [25–28], and coil array [23,29–35] for high and ultrahigh field MR applications in humans. Because of the high frequency property of the microstrip resonator and the behavior of resonator length dependence of the frequency, the microstrip coil design shows challenges in reducing the resonant frequency for heteronuclear MR studies especially for the small animal applications where the coil size is much smaller than that used in humans. The capacitive termination [25,26,29] is one of methods to reduce the resonant frequency. However, in many multinuclear MR studies, the Larmor frequency of the heteronucleus is much lower than that of proton. It often requires impractically large capacitance to tune the resonant frequency down to the Larmor frequency of the heteronucleus in question. This makes its frequency tuning difficult and potentially increases the interaction between proton and heteronuclear channels.

To take advantage of the microstrip resonator and overcome the technical design difficulties facing in practical designs, we propose a design method for dual-tuned quadrature volume coil using a mix of capacitor terminated half-wavelength (λ/2) and quarter-wavelength (λ/4) microstrip resonators for multinuclear MR studies at ultrahigh fields. Compared with λ/2 microstrip resonators, λ/4 resonators with the same physical length operate at significantly lower frequency. This low frequency feature of λ/4 resonators is well suitable for heteronuclear MR applications. To demonstrate the proposed design technique, we have designed a 16-element dual-tuned volume coil in which 8 elements are λ/2 microstrip resonators for ^{1}H channel while another set of 8 elements are λ/4 microstrip resonators for ^{13}C channel. This volume coil is capable of quadrature driving for both ^{13}C channel and ^{1}H channel for improved sensitivity and reduced RF power for spin excitation. The resonant frequency of the λ/4 resonator is only half of that of the λ/2 resonator, therefore the terminated capacitor of the λ/4 resonator for ^{13}C channel can be greatly reduced, making the frequency tuning much easier [36]. The finite-difference time-domain (FDTD) method is used to model the dual-tuned volume coil, determine the capacitance and calculate the B_1 field distributions at the two frequencies. Bench tests and in vivo MR experiments are performed to validate the feasibility and performance of the proposed 7T dual-tuned volume coil design.

2. Materials and methods

2.1 Dual-tuned microstrip volume coil design for ^{1}H and ^{13}C MRI/S

The dual-tuned quadrature microstrip volume coil was designed for ^{1}H imaging and ^{13}C spectroscopy at 7T, corresponding to the resonant frequencies of 298.1 MHz and 75 MHz respectively. A cross-sectional view of the volume coil is shown in Fig.1. There are totally 16 microstrip elements of 8 λ/2 resonators for ^{1}H and 8 λ/4 resonators for ^{13}C equidistantly distributed on a Teflon cylinder which serves as both dielectric substrate and mechanical support. These 8 λ/2 resonators and 8 λ/4 resonators are alternately placed along the Teflon cylinder. Teflon is a low loss dielectric material with loss tangent smaller than 0.0002 and a permittivity of 2.1 at the frequency of interest and has been used as substrate for microstrip surface coil. The dimensions of this cylinder are 6.6cm OD by 5.2 cm ID by 10.1 cm in length. On the inner surface of the Teflon cylinder, 8 microstrip conductors of ^{1}H channel and 8 microstrip conductors of ^{13}C channel were interleaved built. Each microstrip conductor was made from a copper tape with 0.32 cm width and 36 μm thickness (3M, St. Paul, Minnesota). The structure and equivalent circuit of the elements of ^{1}H channel and ^{13}C channel are illustrated in Fig.2 and Fig. 3 respectively, as well as those of the typical microstrip resonator for comparison. For the typical microstrip resonator, the resonant frequency is:

$$f_{element}=\frac{c}{2l\sqrt{\varepsilon_{eff}}} \tag{1}$$

where l and c denote the length of the microstrip conductor and the velocity of light in free space, respectively. ε_{eff} is the effective permittivity of the microstrip resonator.

For the ^{1}H channel, a λ/2 microstrip resonator with capacitive termination on both ends was adopted. The resonant frequency of such a λ/2 resonator can be predicted by solving the following equation [26]:

$$f_{re}=\frac{(2\pi f_{re}Z_0)^2C_{t1}C_{t2}-1}{2\pi Z_0(C_{t1}+C_{t2})}\tan\left(\frac{2\pi l\sqrt{\varepsilon_{eff}}}{c}f_{re}\right) \tag{2}$$

where C_{t1} and C_{t2} are the capacitance of the termination capacitors of the microstrip resonator shown in Fig.2b. Z_0 is the characteristic impedance of the microstrip resonator. Compared with Eq. (1) of the typical microstrip resonator, the resonant frequency can be significantly reduced for the same conductor length l. This enables the microstrip volume coil to be designed for small size coil.

For the ^{13}C channel, a capacitor terminated λ/4 microstrip resonator was adopted. The resonant frequency of such a structure can be deduced by calculating the limitation of the Eq. (2). Thus the resonant frequency of the capacitor terminated λ/4 microstrip resonator can be predicted by solving the following equation:

$$2\pi Z_0C_tf_{re}\tan\left(\frac{2\pi l\sqrt{\varepsilon_{eff}}}{c}f_{re}\right)=1 \tag{3}$$

where C_t is the capacitance of the termination capacitor of the microstrip resonator shown in Fig.2c. Compared with Eq. (2), the resonant frequency can be significantly reduced for the

same capacitance and conductor length. This makes it possible to apply the microstrip resonator to ^{13}C which has a much lower resonant frequency than ^{1}H.

The ground plane of the coil was built by ringing a cylindrical copper foil with 36 μm thickness on the outer surface of the Teflon cylinder. This continuous ground plane can effectively enhance the coupling between the elements.

The resonant frequency of the microstrip volume coil is expressed as [26]:

$$f_{vc}=\frac{1}{\sqrt{1+\frac{1}{L}\sum_{i=1}^{N-1}k_{1,i+1}\cos(\frac{2\pi}{N}i)}}f_{re} \quad (4)$$

where $k_{1,\,i+1}$ is the mutual inductance between the 1st element and the (i+1)th elements, N denotes the number of elements and L denotes the inductance of each microstrip resonant element. In this volume coil design the magnetic coupling dominates the coupling between the elements, therefore the electric coupling was ignored and only mutual inductance to coil induced voltage from the other resonator elements was considered. The resonant element frequency f_{re} denotes that of the ^{1}H channel or the ^{13}C channel. From Eq. (4), it can be seen that the resonant frequency of the volume coil is smaller than that of each element due to the mutual coupling between them.

2.2 FDTD simulations

Based on the structure described above, a coil model was first built and the B_1 field distributions at the two frequencies were numerically simulated using the FDTD. A cylinder-shaped mouse muscle phantom with permittivity of 58 and conductivity of 0.8 was modeled within a 16-element dual-tuned microstrip volume coil. The diameter of the phantom was 4.2 cm which is about 80% of the volume coil ID. Each element of the coil was modeled as a 0.32 cm wide and 10.1 cm long thin strip of copper and placed equal spacing on the surface of a cylinder with 5.2 cm ID, 6.6 cm OD and 10.1 cm length. The permittivity of this cylinder is 2.1, which is the same as that of the Teflon. On the inside surface of this cylinder the ground plane of the volume coil was modeled as a continuous wrapping copper with thickness of 0.36 μm. For the mixed λ/2 resonator of ^{1}H channel, capacitors were connected on both ends of the copper strip as passive load. For the mixed λ/4 resonator of ^{13}C channel, on one end the strip was directly connected to the ground plane using a copper strip with the same width of the strip; on the other end a capacitor was connected between the strip and the ground using a perfect electric conductor. The coaxial cable of the volume coil was modeled as a series voltage source with 50 ohm impedance which was connected to each driven port of the coil model. Linear drive was used for each channel. The Yee cell was 1 mm which was small enough for satisfying the simulation accuracy. The Gauss waveform was used to determine the value of the terminated capacitors and the stop criteria were that the calculation converged to −35 dB or reached the maximum iteration number of 10^6. Then, the Sine waveform was used to calculate the B_1 field distributions and the stop criteria were that the calculation converged to −40 dB or the iteration number reached 300,000. All the FDTD calculation was performed using the software XFDTD 6.4 (Remcom, Inc.) on a PC with 2.33 GHz CPU and 4 GB memory.

To investigate the RF efficiency and field homogeneity of our proposed design, a conventional 16-strut dual-tuned birdcage coil was modeled and compared with the microstrip coil model. The conventional birdcage was in the same size as the microstrip coil: the diameter was 5.2 cm and the length was 10.1 cm. 8 struts of ^{1}H channel and 8 struts of ^{13}C channel were alternately placed. Each strut was made from a copper tape with 0.32

cm width and 36 um thickness (3M, St. Paul, Minnesota). The capacitor value for ^{1}H channel was 7.4 pF while that for ^{13}C channel was 59 pF. The same phantom was modeled within the coil. All the other settings for the FDTD simulation were kept the same.

2.3 Bench test

Based on the simulation results, a dual-tuned microstrip volume coil for ^{1}H and ^{13}C was then built as shown in Fig.4. To generate a circularly polarized B_1 field, the coil operated in quadrature with connection to a 3-dB 90° quadrature hybrid. In both ^{1}H and ^{13}C channels, two driving elements of the volume coil were 90° apart in phase. The frequency tuning of the two channels can be achieved by adjusting the termination capacitors. The impedance matching of the volume coil can be achieved by varying the trimmer capacitor (Voltronics, Denville, NJ) which was connected in series to the microstrip conductors of the driving element.

An Agilent E5070B network analyzer was used for testing the coil resonance modes, the isolation between two quadrature ports and that between the proton and carbon channels. As shown in Fig.1, there are totally 4 ports on the dual-tuned volume coil: 0° ^{1}H port, 90° ^{1}H port, 0° ^{13}C port and 90° ^{13}C port. The resonance modes of the 4 ports were tested using the reflection parameter S_{11} firstly. Then the isolation between two pair of quadrature ports of ^{1}H channel and ^{13}C channel were tested using the transmission parameter S_{21}. To test the isolation between the ^{1}H and ^{13}C channels, the S_{21} between them was also measured at both resonant frequencies.

2.4 Phantom and in vivo MRI

Both phantom and in vivo images were tested using a commercial 7T General Electric Signa™ scanner. In the phantom experiment, the ^{1}H images and ^{13}C spectroscopic images of a cylindrical corn coil phantom were obtained in axial plane. The ^{1}H image of the phantom was acquired using a gradient echo (GRE) sequence with FOV =10 cm, encoding matrix = 256×128, slice thickness = 3 mm, TR= 100 ms, TE= 6.8 ms, FA = 30° and Average number = 1. The ^{13}C spectroscopic image was acquired using the FIDCSI sequence (GE Healthcare, Waukesha, WI, USA) with TR = 2 sec, 10 mm in plane slice and 20 mm thickness. The FIDCSI is 2D chemical shift imaging by using a set of phase-encoded free induction decay signals. A proton image of a mouse was also acquired in sagittal plane using a fast spin echo (FSE) sequence with the following imaging parameters: FOV = 9 cm, encoding matrix = 192×192, slice thickness = 1.6 mm, TR= 4000 ms, TE= 104.08 ms, FA = 90° and Average number = 1.

3. Results

3.1 simulations

Theoretical calculation based on the analytical equations was first applied to estimate the capacitance for each element of the ^{1}H and ^{13}C channel. Then these estimated capacitances were used to build the numerical model for the dual-tuned microstrip volume coil in xFDTD environment and the Gauss waveform was used to sweep frequency to determine the value of each capacitor. After several iterations, proper capacitances were found: for the λ/2 resonator in ^{1}H channel the terminated capacitors are 13.6 pF and 6.8 pF, and for the λ/4 resonator in ^{13}C channel the terminated capacitance was 70 pF. Using this setting, the *sine* waveform was used to calculate the B_1 field distribution of each channel. Both the ^{1}H channel and ^{13}C channel generate a homogeneous RF field within the interested area of the phantom. As shown in Fig.5a, when the 298.1 MHz *sine* wave signal was input into the driven port of the ^{1}H channel, the elements of the ^{1}H channel were all excited except the elements which were orthogonal to the driven element, while all the elements of the ^{13}C

channel were suppressed. When the 75 MHz Sine waveform was used, the ^{13}C channel excited and the ^{1}H channel was quiet, which is shown in Fig.6a. The sinusoid distributions of the currents for both ^{1}H and ^{13}C channels along the circumference of the coil are clearly illustrated. These results show excellent isolation between ^{1}H and ^{13}C channels, which is desired in dual-tuned RF coil design.

Fig.5b shows the RF field distribution of the ^{1}H channel of the 16-strut dual-tuned birdcage coil. Compared with Fig.5a, the RF field of the birdcage coil used in this work is slightly weaker than that of the microstrip. The 1D plot in Fig.5c shows this difference more clearly. The RF efficiency of the ^{1}H channel of the microstrip volume coil is approximately 1 dB higher than that of the birdcage coil, while the homogeneity variation of both coils are within 1.8 dB range. As a comparison of Fig.6a which shows the ^{13}C RF field distribution of the microstrip volume coil, Fig.6b shows that of the conventional birdcage coil. The 1D plot in Fig.6c illustrates that, in this specific case, the RF efficiency of the ^{13}C channel of the microstrip volume coil is approximately 6 dB higher than that of the birdcage coil, while the homogeneity variation of the two coils are both within 1 dB range.

3.2 Bench test

The resonance modes of one driving port of ^{1}H channel and the isolation between the two driving ports were plotted in Fig.6. When ^{1}H channel were tuned at 298.1 MHz, the reflection coefficient S_{11} of the two ports are both better than −43 dB, and the transmission coefficient S_{21} between the two quadurature ports is −26 dB. Fig.7 shows the resonance modes and the isolation between the two quadrature ports of the ^{13}C channel when tuned at 74.94 MHz. The reflection coefficient S_{11} of the two ports are better than −32 dB, while the transmission coefficient S_{21} between the two quadurature ports is better than −27 dB. These results ensure excellent quadrature performance of both ^{1}H and ^{13}C channels.

The isolation between the ^{1}H channel and the ^{13}C channel is illustrated in Fig.8. The transmission coefficient S_{21} between two channels was plotted at both 74.94 MHz and 298.1 MHz with 30 MHz span. Also, the S_{21} from 50 MHz to 330 MHz span is shown. The S_{21} at 74.94 MHz is better than −50 dB and that at 298.1 MHz is better than −35 dB, indicating that the two channels of ^{1}H and ^{13}C are isolated sufficiently, which is essential for efficient acquisition of ^{13}C MR signals.

Based on the simulation results and bench tests, the capacitance C_{t1} and C_{t2} on the ^{1}H element were 12.4 pF and 6.8 pF respectively. The capacitance C_t on the ^{13}C element was 68 pF and a variable capacitor (Johneson9620, 0.5 – 2.5 pF) was parallel connected into the element to perform frequency tuning.

3.3 MRI tests

After B_0 shimming using the ^{1}H channel MR tests was performed. The ^{1}H GRE image and ^{13}C spectroscopic image in the axial plane of a corn oil phantom was acquired sequentially and are shown in Fig.9. These two images illustrate high quality of proton image and carbon spectroscopic image of the microstrip volume coil. The chemical shift artifacts of the oil phantom at the ultrahigh field of 7T are also clearly observed in this image. Another proton in vivo image of a mouse on sagittal plane shown is also shown in Fig.10. This demonstrates that the proposed dual-tuned volume coil design can provide a fairly homogeneous B_1 field and image coverage with loading in the 300MHz range.

4. Discussion and Conclusion

A novel design for dual-tuned quadrature volume coil using a mix of capacitor terminated half-wavelength and quarter-wavelength microstrip resonators for multinuclear MR studies

at 7T has been proposed. An example volume coil design for $^{1}H/^{13}C$ spectroscopic imaging for mouse study has been presented to demonstrate the feasibility of this method. High quality proton image and carbon spectroscopic image of a corn oil phantom have been obtained using this dual-tuned microstrip volume coil. Both simulations and MR experiment results have shown the excellent performance of the proposed design method.

In this design, mixed λ/2 and λ/4 resonators were utilized to fit the different resonant frequencies of ^{1}H and ^{13}C respectively. At the same length, λ/4 resonators operate at relatively low frequency compared with the commonly used λ/2 resonators in RF coil design. Therefore, the use of λ/4 resonators is advantageous for ^{13}C channel and makes it much convenient to perform frequency tuning by using commercially available variable capacitors.

The FDTD simulation has shown that the dual-tuned microstrip volume coil can generate homogeneous B_1 fields at both ^{1}H and ^{13}C resonant frequencies. When the elements of one frequency are excited there is nearly no signal in the elements of the other frequency, showing excellent isolation between the two channels, which is desired in dual-tuned RF coil designs because it can help to increase efficiency of heteronuclear MR signal excitation and detection. Quadrature driving has been applied to both the ^{1}H and ^{13}C channels of the volume coil to improve the SNR and reduce RF excitation power. The transmission parameters S_{21} between each pair of driving ports of ^{1}H and ^{13}C channels are −26 dB and −27 dB respectively, ensuring excellent quadrature performance of both ^{1}H and ^{13}C channels. Measured on a network analyzer, the transmission parameters S_{21} between a driving port of ^{1}H and that of ^{13}C is better than −50 dB at 75 MHz and −35 dB at 298.1 MHz. This measured result demonstrates that the ^{1}H and ^{13}C channels have been isolated excellently and is in agreement with the FDTD simulation results. In summary, this dual-tuned microstrip volume coil with mixed λ/2 and λ/4 resonant elements is feasible and efficient, provided that sufficient radial separation is maintained between the strip conductor and the ground to provide sufficient coupling between elements. The characteristic of the microstrip provides a simple approach to design dual-tuned volume coil for in vivo multinuclear MR at ultrahigh fields.

Acknowledgments

This work was partially supported by NIH grants EB004453, EB008699 and EB007588-03S1, and a QB3 Research Award.

References

1. de Graaf RA, Mason GF, Patel AB, Behar KL, Rothman DL. In vivo 1H-[13C]-NMR spectroscopy of cerebral metabolism. NMR Biomed. 2003; 16(6–7):339–357. [PubMed: 14679499]
2. Gruetter R, Adriany G, Choi IY, Henry PG, Lei H, Oz G. Localized in vivo 13C NMR spectroscopy of the brain. NMR Biomed. 2003; 16(6–7):313–338. [PubMed: 14679498]
3. Henry PG, Tkac I, Gruetter R. 1H-localized broadband 13C NMR spectroscopy of the rat brain in vivo at 9.4 T. Magn Reson Med. 2003; 50(4):684–692. [PubMed: 14523952]
4. Kurhanewicz J, Bok R, Nelson SJ, Vigneron DB. Current and potential applications of clinical 13C MR spectroscopy. J Nucl Med. 2008; 49(3):341–344. [PubMed: 18322118]
5. Li S, Zhang Y, Wang S, Yang J, Ferraris Araneta M, Farris A, et al. In vivo 13C magnetic resonance spectroscopy of human brain on a clinical 3 T scanner using [2-13C]glucose infusion and low-power stochastic decoupling. Magn Reson Med. 2009; 62(3):565–573. [PubMed: 19526500]
6. Boada FE, Gillen JS, Shen GX, Chang SY, Thulborn KR. Fast three dimensional sodium imaging. Magn Reson Med. 1997; 37(5):706–715. [PubMed: 9126944]

7. Thulborn KR, Davis D, Snyder J, Yonas H, Kassam A. Sodium MR imaging of acute and subacute stroke for assessment of tissue viability. Neuroimaging Clin N Am. 2005; 15(3):639–653. xi–xii. [PubMed: 16360594]
8. Constantinides CD, Kraitchman DL, O'Brien KO, Boada FE, Gillen J, Bottomley PA. Noninvasive quantification of total sodium concentrations in acute reperfused myocardial infarction using 23Na MRI. Magn Reson Med. 2001; 46(6):1144–1151. [PubMed: 11746581]
9. Ugurbil K, Kingsley-Hickman PB, Sako EY, Zimmer S, Mohanakrishnan P, Robitaille PM, et al. 31P NMR studies of the kinetics and regulation of oxidative phosphorylation in the intact myocardium. Ann N Y Acad Sci. 1987; 508:265–286. [PubMed: 2964217]
10. Lei H, Zhu XH, Zhang XL, Ugurbil K, Chen W. In vivo 31P magnetic resonance spectroscopy of human brain at 7 T: an initial experience. Magn Reson Med. 2003; 49(2):199–205. [PubMed: 12541238]
11. Hetherington HP, Kim JH, Pan JW, Spencer DD. 1H and 31P spectroscopic imaging of epilepsy: spectroscopic and histologic correlations. Epilepsia. 2004; 45 Suppl 4:17–23. [PubMed: 15281952]
12. Rothman DL, Shulman RG, Shulman GI. 31P nuclear magnetic resonance measurements of muscle glucose-6-phosphate. Evidence for reduced insulin-dependent muscle glucose transport or phosphorylation activity in non-insulin-dependent diabetes mellitus. J Clin Invest. 1992; 89(4): 1069–1075. [PubMed: 1556176]
13. Chew WM, Moseley ME, Nishimura MC, Hashimoto T, Pitts LH, James TL. A novel double-surface coil approach to phosphorus-31 spectroscopy: a study of hemispheric brain injury in the rat. Magn Reson Med. 1985; 2(6):567–575. [PubMed: 3880098]
14. Shen GX, Boada FE, Thulborn KR. Dual-frequency, dual-quadrature, birdcage RF coil design with identical B1 pattern for sodium and proton imaging of the human brain at 1.5 T. Magn Reson Med. 1997; 38(5):717–725. [PubMed: 9358445]
15. Shen GX, Wu JF, Boada FE, Thulborn KR. Experimentally verified, theoretical design of dual-tuned, low-pass birdcage radiofrequency resonators for magnetic resonance imaging and magnetic resonance spectroscopy of human brain at 3.0 Tesla. Magn Reson Med. 1999; 41(2):268–275. [PubMed: 10080273]
16. Amari S, Ulug AM, Bornemann J, van Zijl PC, Barker PB. Multiple tuning of birdcage resonators. Magn Reson Med. 1997; 37(2):243–251. [PubMed: 9001149]
17. Matson GB, Vermathen P, Hill TC. A practical double-tuned 1H/31P quadrature birdcage headcoil optimized for 31P operation. Magn Reson Med. 1999; 42(1):173–182. [PubMed: 10398964]
18. Rath AR. Design and Performance of a Double-Tuned Bird-Cage Coil. Journal of Magnetic Resonance. 1990; 86(3):488–495.
19. Vaughan JT, Hetherington HP, Otu JO, Pan JW, Pohost GM. High frequency volume coils for clinical NMR imaging and spectroscopy. Magn Reson Med. 1994; 32(2):206–218. [PubMed: 7968443]
20. Zhang, X.; Zhu, X.; Qiao, H.; Liu, H.; Vaughan, JT.; Ugurbil, K., et al. A circular-polarized double-tuned (31P and 1H) TEM coil for human head MRI/MRS at 7T. Toronto: 2003. p. 423
21. Avdievich NI, Hetherington HP. 4 T Actively detuneable double-tuned 1H/31P head volume coil and four-channel 31P phased array for human brain spectroscopy. J Magn Reson. 2007; 186(2): 341–346. [PubMed: 17379554]
22. Pang Y, Zhang X, Xie Z, Wang C, Vigneron D. Common-mode differential-mode (CMDM) method for double-nuclear MR signal excitation and reception at ultrahigh fields. IEEE Trans Med Imaging. 2011 Jun 20. Epub ahead of print.
23. Lee RF, Westgate CR, Weiss RG, Newman DC, Bottomley PA. Planar strip array (PSA) for MRI. Magn Reson Med. 2001; 45(4):673–683. [PubMed: 11283996]
24. Zhang X, Ugurbil K, Chen W. Microstrip RF surface coil design for extremely high-field MRI and spectroscopy. Magn Reson Med. 2001; 46(3):443–450. [PubMed: 11550234]
25. Zhang X, Ugurbil K, Chen W. A microstrip transmission line volume coil for human head MR imaging at 4T. J Magn Reson. 2003; 161(2):242–251. [PubMed: 12713976]
26. Zhang X, Ugurbil K, Sainati R, Chen W. An inverted-microstrip resonator for human head proton MR imaging at 7 tesla. IEEE Trans Biomed Eng. 2005; 52(3):495–504. [PubMed: 15759580]

27. Zhang X, Zhu XH, Chen W. Higher-order harmonic transmission-line RF coil design for MR applications. Magn Reson Med. 2005; 53(5):1234–1239. [PubMed: 15844152]

28. Pang Y, Xie Z, Li Y, Xu D, Vigneron D, Zhang X. Resonant mode reduction in radiofrequency volume coils for ultrahigh field magnetic resonance imaging. Materials. 2011; 4(8):1333–1344. [PubMed: 22081791]

29. Wu B, Zhang X, Qu P, Shen GX. Design of an inductively decoupled microstrip array at 9.4 T. J Magn Reson. 2006; 182(1):126–132. [PubMed: 16829145]

30. Wu B, Zhang X, Qu P, Shen GX. Capacitively decoupled tunable loop microstrip (TLM) array at 7 T. Magn Reson Imaging. 2007; 25(3):418–424. [PubMed: 17371734]

31. Adriany G, Van de Moortele PF, Wiesinger F, Moeller S, Strupp JP, Andersen P, et al. Transmit and receive transmission line arrays for 7 Tesla parallel imaging. Magn Reson Med. 2005; 53(2): 434–445. [PubMed: 15678527]

32. Wu B, Wang C, Kelley DA, Xu D, Vigneron DB, Nelson SJ, et al. Shielded microstrip array for 7T human MR imaging. IEEE Trans Med Imaging. 2010; 29(1):179–184. [PubMed: 19822470]

33. Wu B, Wang C, Krug R, Kelley DA, Xu D, Pang Y, et al. 7T human spine imaging arrays with adjustable inductive decoupling. IEEE Trans Biomed Eng. 2010; 57(2):397–403. [PubMed: 19709956]

34. Adriany G, Auerbach EJ, Snyder CJ, Gozubuyuk A, Moeller S, Ritter J, et al. A 32-channel lattice transmission line array for parallel transmit and receive MRI at 7 tesla. Magn Reson Med. 2010; 63(6):1478–1485. [PubMed: 20512850]

35. Metzger GJ, van de Moortele PF, Akgun C, Snyder CJ, Moeller S, Strupp J, et al. Performance of external and internal coil configurations for prostate investigations at 7 T. Magn Reson Med. 2010; 64(6):1625–1639. [PubMed: 20740657]

36. Xie, Z.; Xu, D.; Kelley, D.; Vigneron, D.; Zhang, X. A dual-tuned quadrature microstrip volume coil for 13C/1H MRI/S at 7T. Toronto: 2008. p. 1113

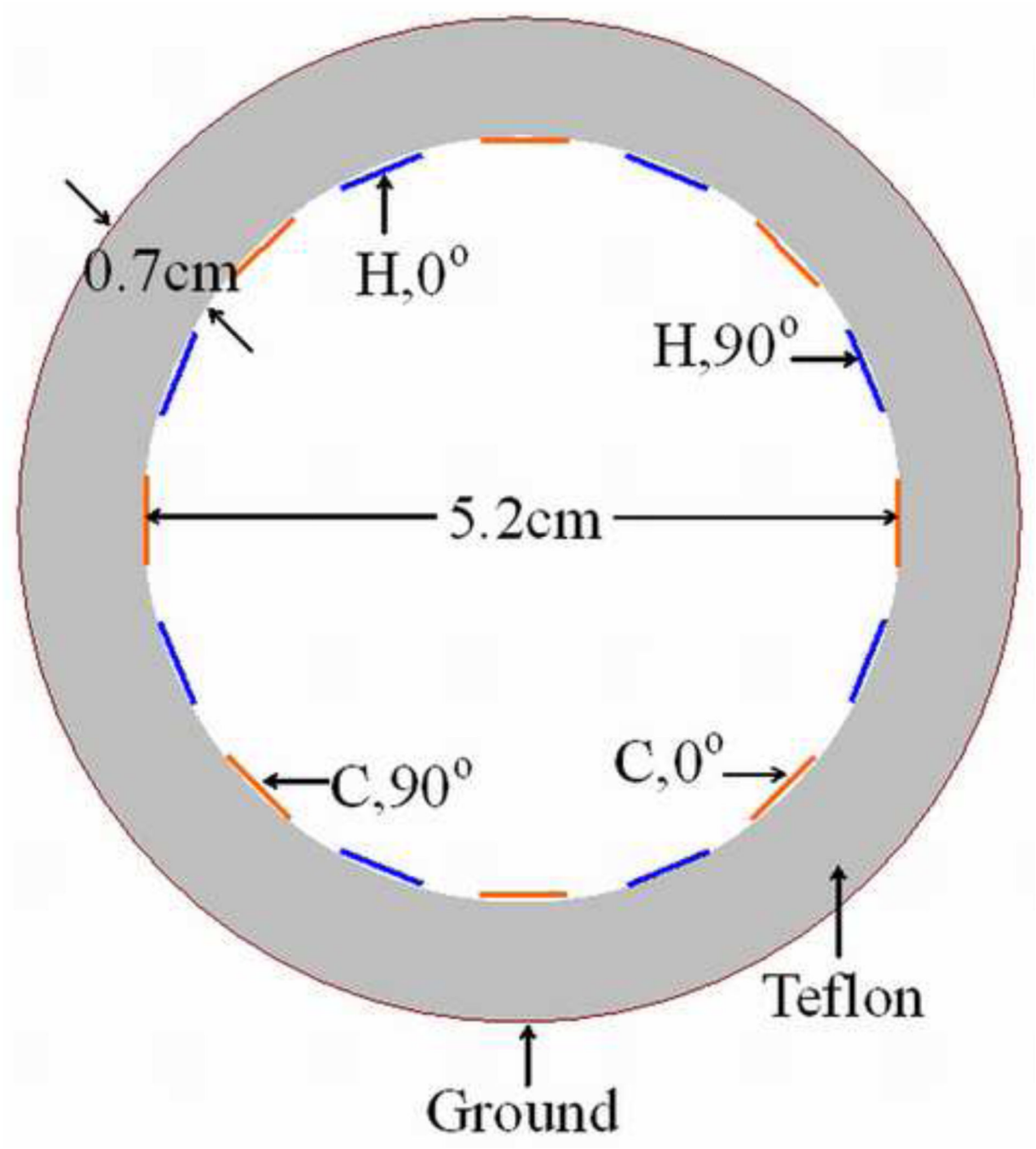

Figure 1.
The cross-sectional view of the dual-tuned quadrature microstrip volume coil with mixed λ/2 and λ/4 resonators. The λ/2 and λ/4 resonators are alternately arranged along the circumference of the cylindrical volume coil. With this structure, both channels can be driven in quadrature for improved SNR and reduced excitation power.

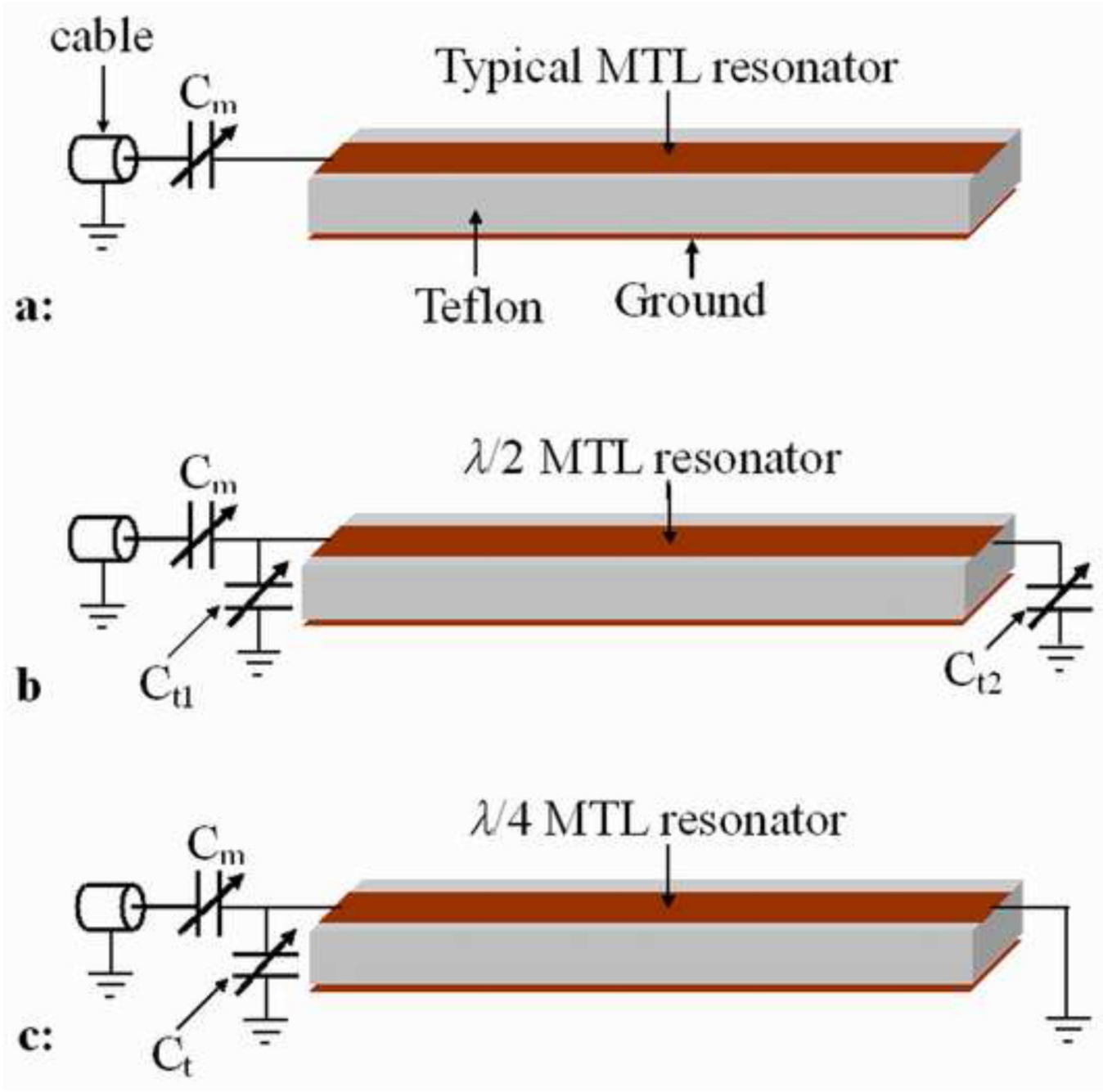

Figure 2.
Diagrams of (a) typical open-circuited MTL resonator, (b) capacitor terminated λ/2 MTL resonator and (c) capacitor terminated λ/4 MTL resonator.

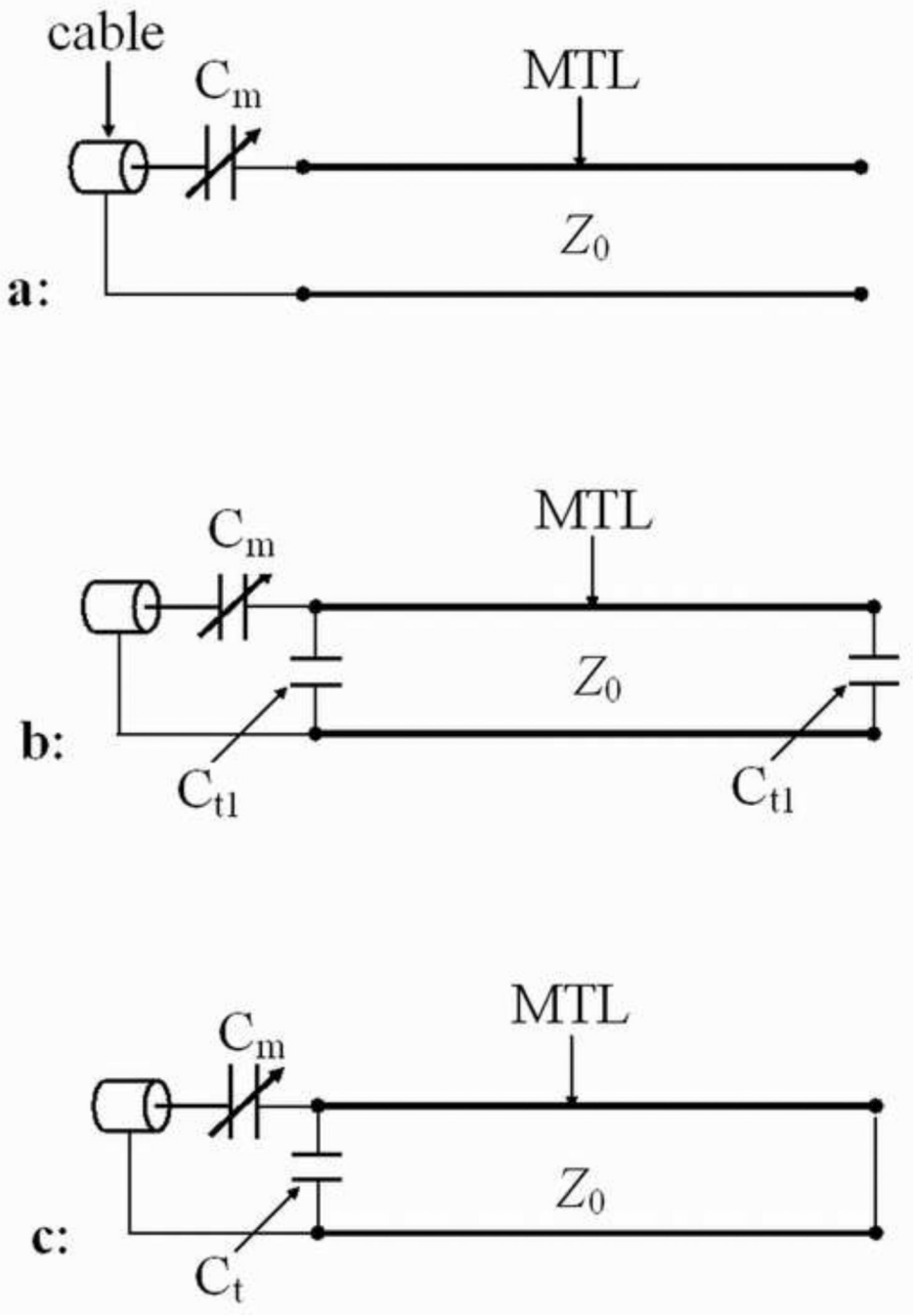

Figure 3.
Equivalent circuits of (a) the typical open-circuited MTL resonator, (b) capacitor terminated λ/2 MTL resonator and (c) capacitor terminated λ/4 MTL resonator.

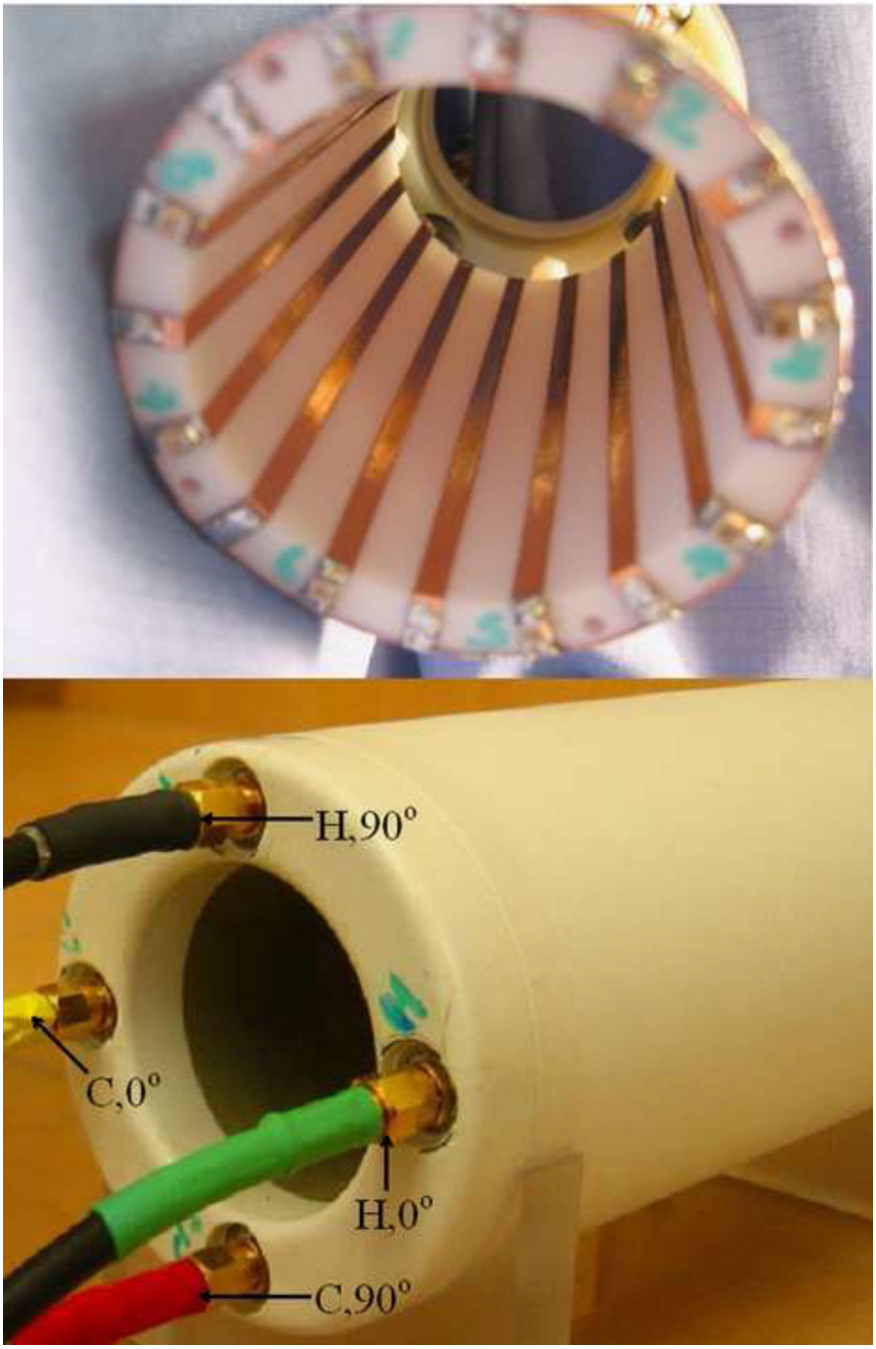

Figure 4.
(a) Structure of the proposed 8-element by 8-element dual-tuned volume coil using alternately placed λ/2 and λ/4 microstrip resonators for in vivo $^{13}C/^{1}H$ MRSI applications at 7T and (b) Prototype of this dual-tuned microstrip volume coil with two sets of quadrature feedings.

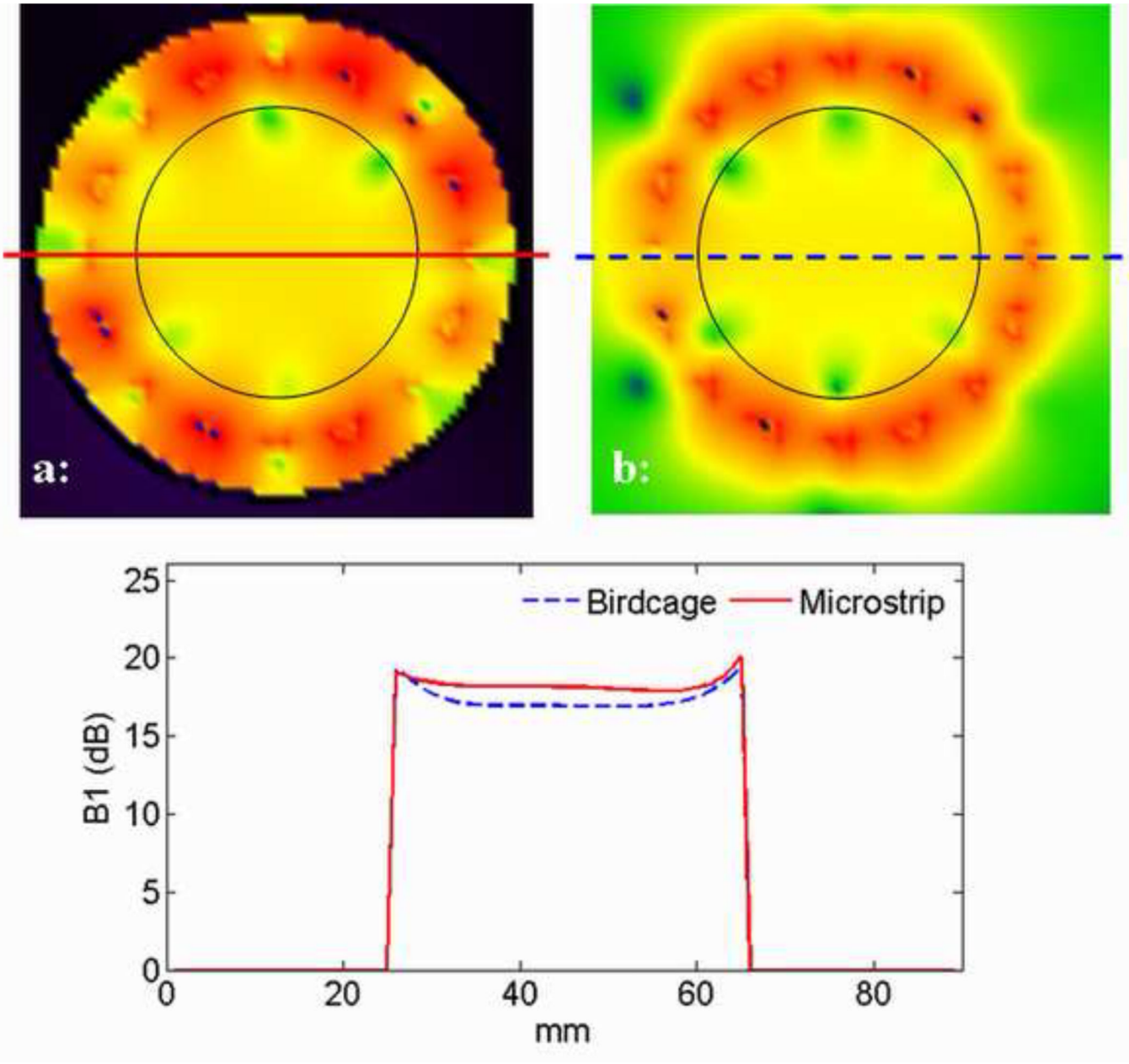

Figure 5.

B_1 field distributions of the ^{1}H channel of (a) microstrip dual-tuned volume coil and (b) conventional dual-tuned birdcage coil calculated using FDTD method. (c) 1D plot of the field distribution along the central line of the 2D images. The red line denotes the microstrip coil while the blue line denotes the birdcage coil. The RF efficiency of the microstrip coil is around 1 dB higher than that of the birdcage coil, while the homogeneity variation of both coils is within 1.8 dB range.

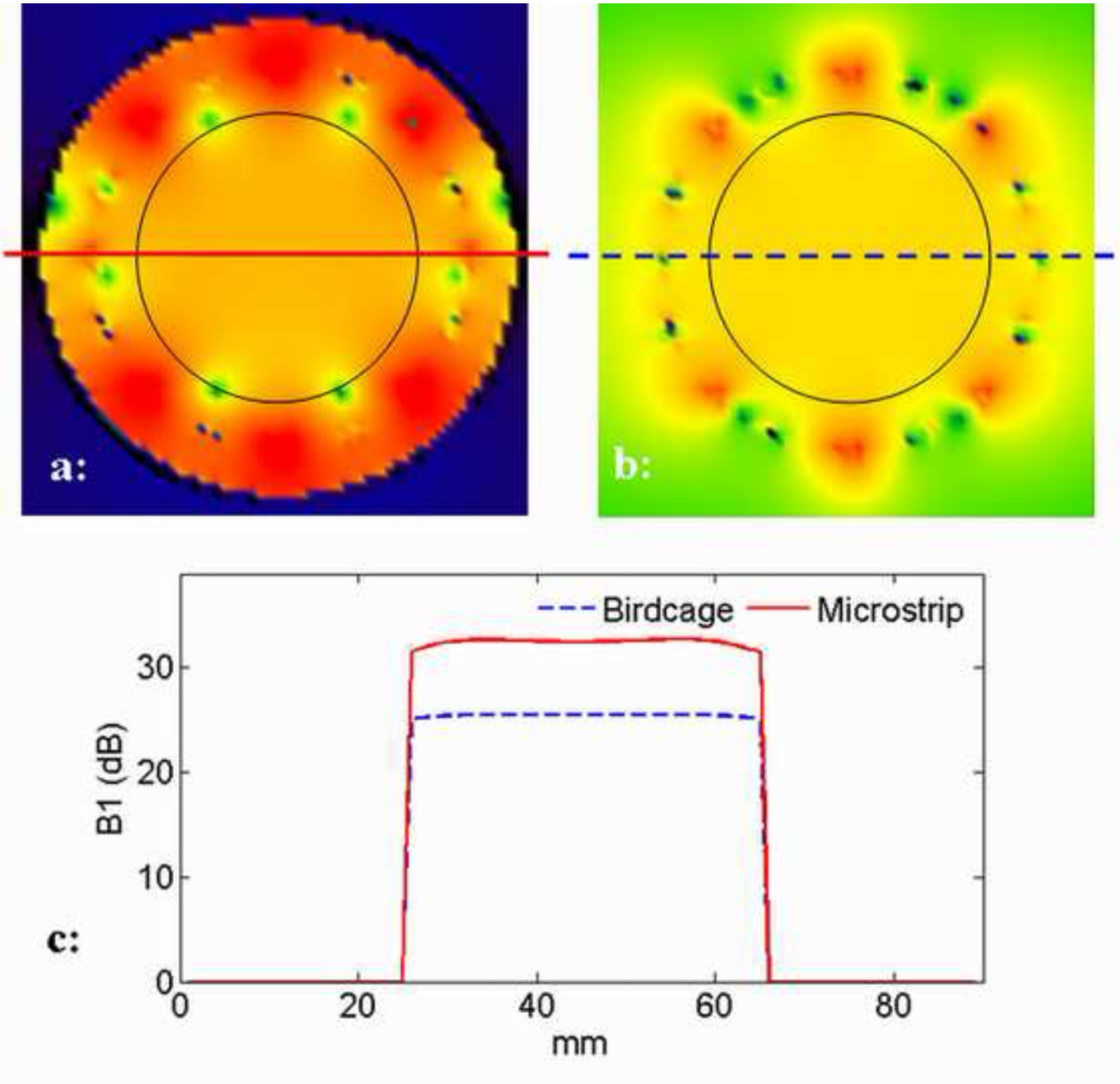

Figure 6.

B_1 field distributions of the ^{13}C channel of (a) microstrip dual-tuned volume coil and (b) conventional dual-tuned birdcage coil calculated using FDTD method. (c) 1D plot of the field distribution along the central line of the 2D images. The red line denotes the microstrip coil while the blue line denotes the birdcage coil. The RF efficiency of the ^{13}C channel of the microstrip coil is around 6 dB higher than that of the birdcage coil, while the homogeneity variation of both coils is within 1 dB range.

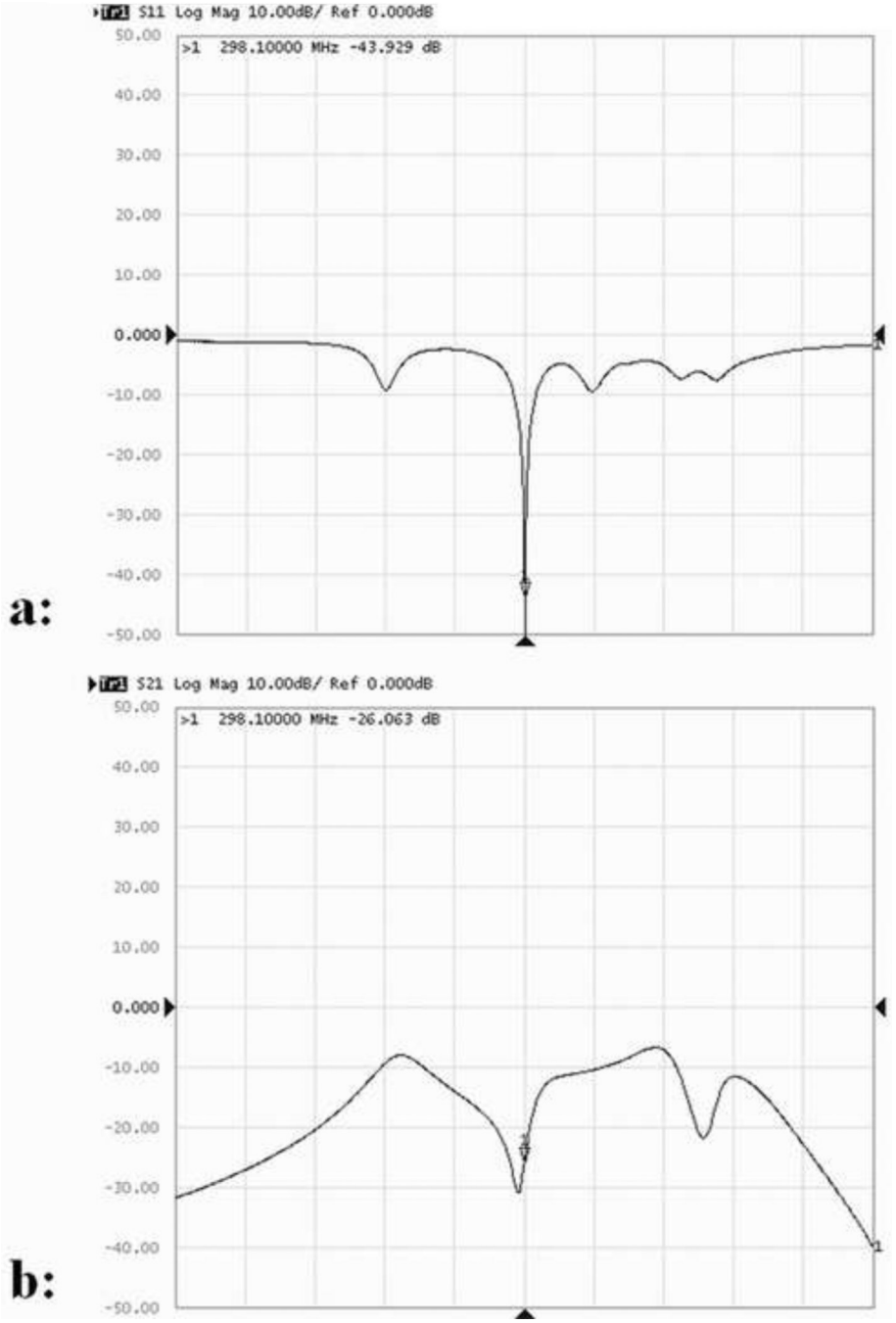

Figure 7.

(a) S_{11} plot of one driving port of ^1H channel showing the multimodal behavior of the dual-tuned volume coil with 8 ^1H elements; (b) S_{21} measurement of the two driving ports of ^1H channel, indicating the accuracy of the 900 phase requirement of the two quadrature ports in the 300 MHz range.

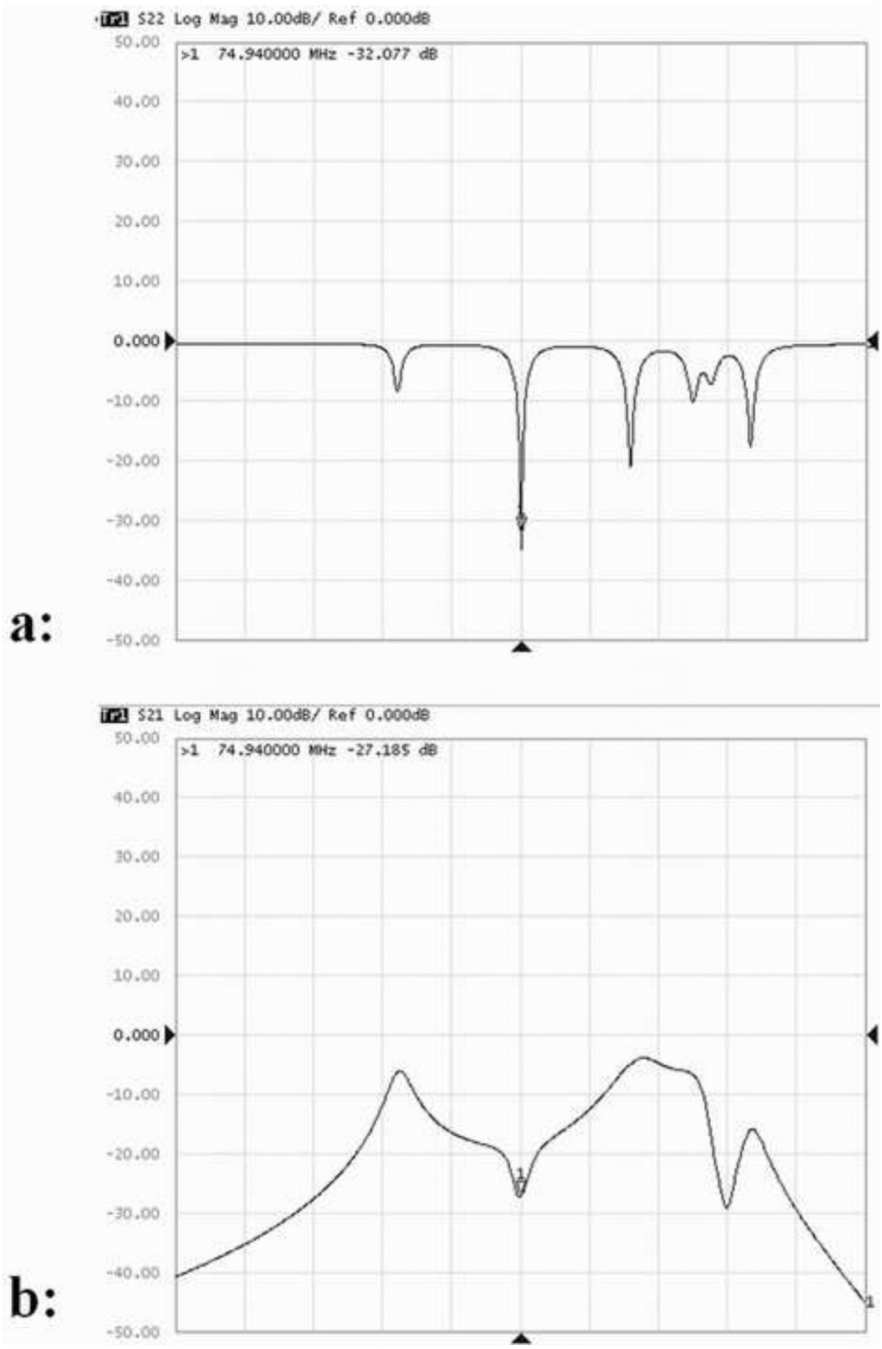

Figure 8.

(a) S_{11} plot of one driving port of ^{13}C channel, showing the well-defined resonance modes of the dual-tuned coil with 8 elements; (b) S_{21} measurement between the two quadrature driving ports of ^{13}C channel. The sufficient isolation (~27dB) indicates accuracy of the 90° phase requirement of the two quadrature ports.

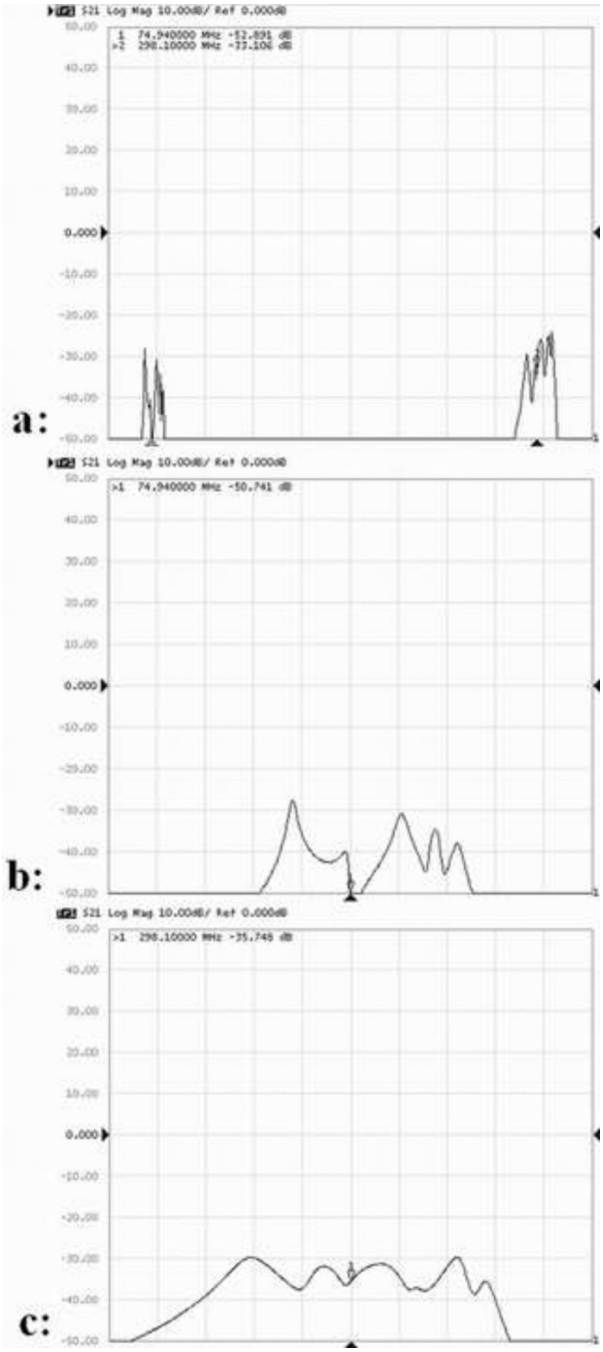

Figure 9.

S_{21} measurements between the ^{13}C channel and the ^{1}H channel (a) in frequency ranges of 50 – 330 MHz, (b) 75 MHz and (c) 298.1 MHz. Sufficient electromagnetic isolation between ^{13}C channel and ^{1}H channel of the proposed dual-tuned volume coil is essential for efficient acquisition of ^{13}C signals.

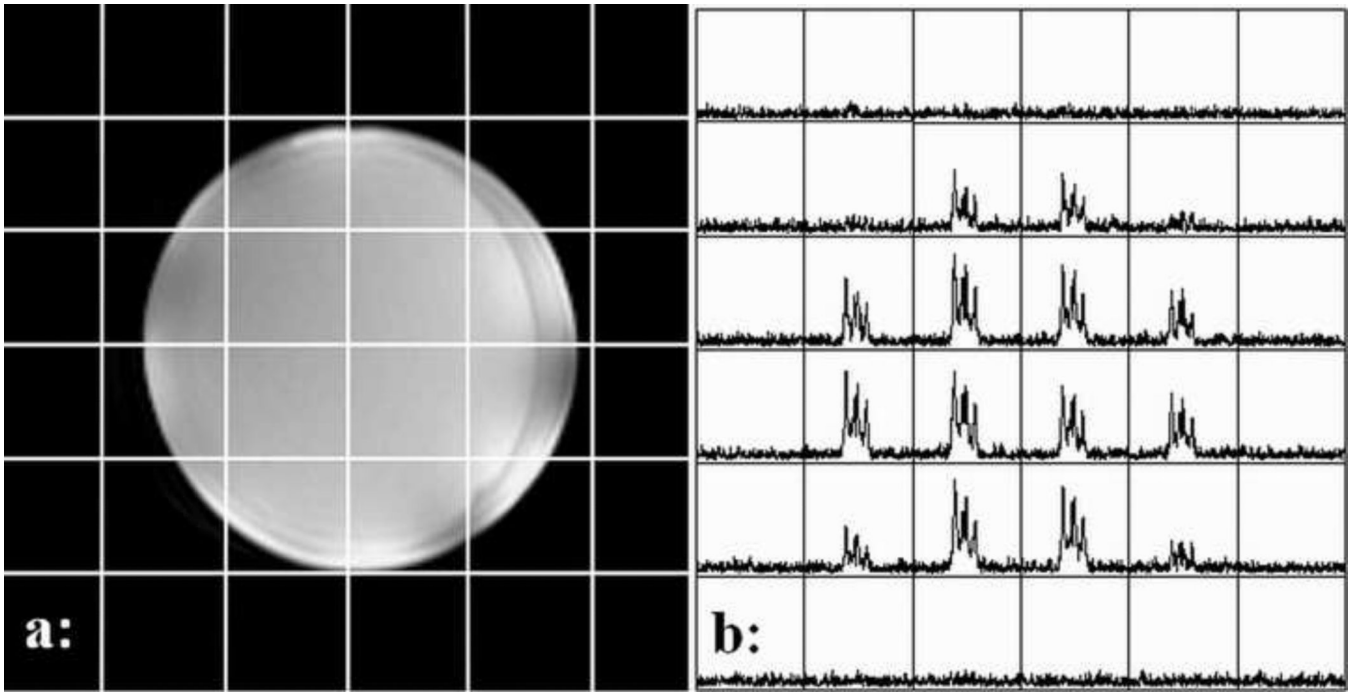

Figure 10.
MR images of the dual-tuned microstrip volume coil at 7T: (a) ^{1}H image of a corn oil phantom on axial plane (chemical shift artifacts of the oil phantom at the ultrahigh field of 7T are clearly observed in this image); (b) ^{13}C FIDCSI spectroscopic image of the corn oil phantom (with natural abundance) on axial plane.

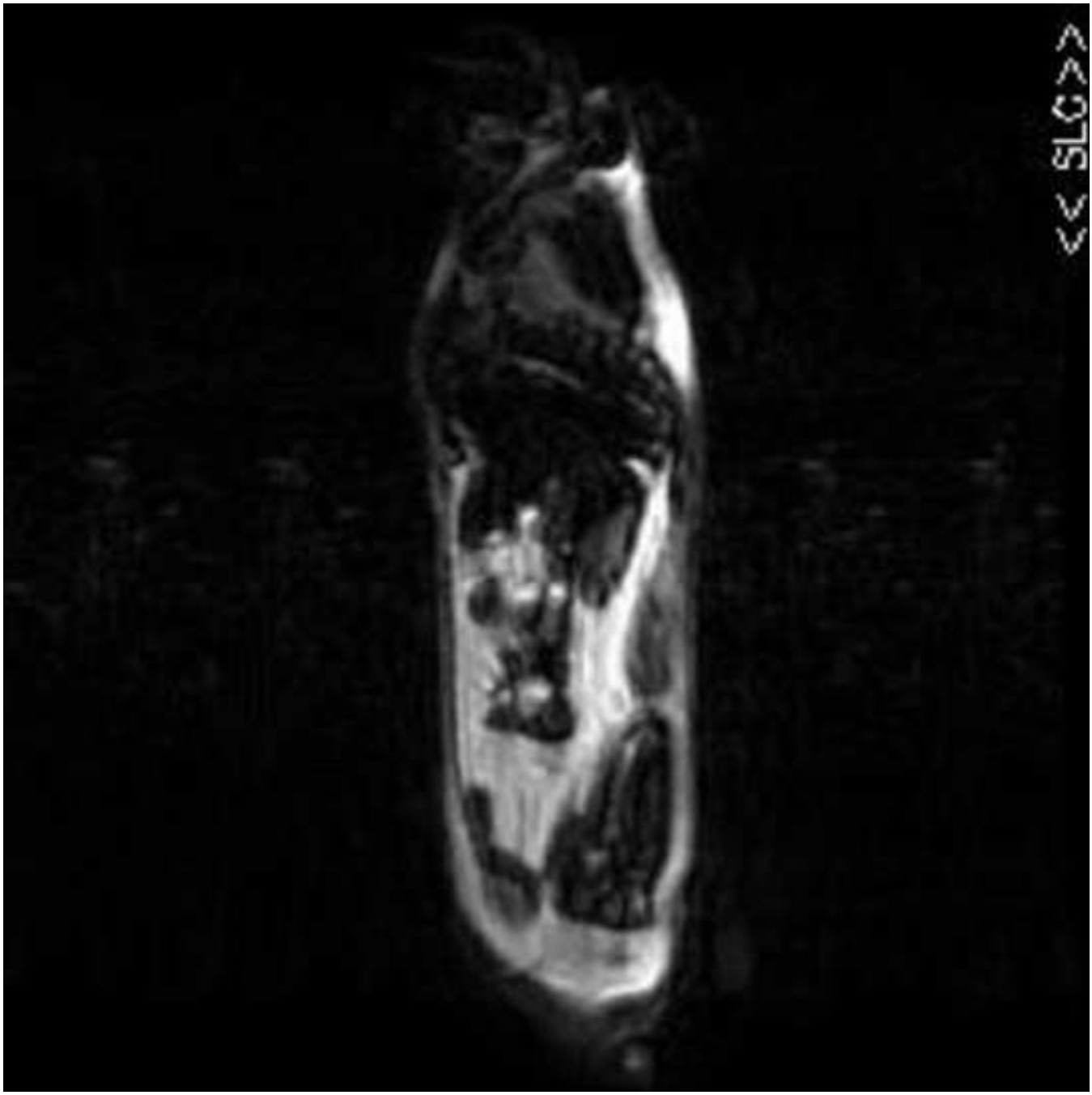

Figure 11.

^{1}H in vivo image of a mouse on sagittal plane acquired using the ^{1}H channel of the proposed dual-tuned volume coil at 7T. This preliminary ^{1}H imaging result demonstrates that the proposed dual-tuned volume coil design can provide a fairly homogeneous B_1 field and image coverage with loading in the 300MHz range.